JOURNAL OF GEOPHYSICAL RESEARCH, VOL. 111, B09203, doi:10.1029/2005JB004052, 2006

Single-crystal elasticity and sound velocities of $(Mg_{0.94}Fe_{0.06})O$ ferropericlase to 20 GPa

Jennifer M. Jackson,[1,2] Stanislav V. Sinogeikin,[1,3] Steven D. Jacobsen,[4,5] Hans J. Reichmann,[6] Stephen J. Mackwell,[7] and Jay D. Bass[1]

Received 15 September 2005; revised 25 January 2006; accepted 6 March 2006; published 7 September 2006.

[1] The single-crystal elastic properties of high-spin $(Mg_{0.94}Fe_{0.06})O$ ferropericlase were measured by Brillouin spectroscopy on a sample compressed to 20 GPa with diamond anvil cells using methanol-ethanol-water as a pressure-transmitting medium. At room pressure, the adiabatic bulk (K_{0S}) and shear (μ_{0S}) moduli are $K_{0S} = 163 \pm 3$ GPa and $\mu_{0S} = 121 \pm 2$ GPa, in excellent agreement with ultrasonic results from the same bulk sample (Jacobsen et al., 2002). A fit to all our high-pressure Brillouin data using a third-order finite-strain equation of state yields the following pressure derivatives of the adiabatic bulk and shear moduli: $K'_{0S} = 3.9 \pm 0.2$ and $\mu'_{0S} = 2.1 \pm 0.1$. Within the uncertainties, we find that K_{0S} and K'_{0S} of $(Mg_{0.94}Fe_{0.06})O$ are unchanged from MgO. However, μ_{0S} and μ'_{0S} of $(Mg_{0.94}Fe_{0.06})O$ are reduced by 8% and 11%, respectively. The aggregate compressional (V_P) and shear (V_S) wave velocities are reduced by 4% and 6%, respectively, as compared to MgO. The pressure dependence of the single-crystal elastic moduli and aggregate sound velocities is linear within the investigated pressure range. The elastic anisotropy of $(Mg_{0.94}Fe_{0.06})O$ is about 10% greater than that of MgO at ambient conditions. At the highest pressure obtained here, the elastic anisotropy of $(Mg_{0.94}Fe_{0.06})O$ is close to zero. On the basis of our measurements and earlier ultrasonic measurements, we find that the pressure derivatives of shear moduli obtained at room pressure for low iron concentrations (<20 mol% FeO) of high-spin ferropericlase are inconsistent with those inferred from the lower mantle PREM model.

Citation: Jackson, J. M., S. V. Sinogeikin, S. D. Jacobsen, H. J. Reichmann, S. J. Mackwell, and J. D. Bass (2006), Single-crystal elasticity and sound velocities of $(Mg_{0.94}Fe_{0.06})O$ ferropericlase to 20 GPa, *J. Geophys. Res.*, *111*, B09203, doi:10.1029/2005JB004052.

1. Introduction

[2] Ferropericlase, (Mg,Fe)O, is expected to coexist with aluminous ferromagnesian silicate perovskite and calcium silicate perovskite in Earth's lower mantle (660–2900 km depth) [*Anderson and Bass*, 1986; *Knittle and Jeanloz*, 1987; *Irifune*, 1994; *Fiquet et al.*, 2000; *Shim et al.*, 2000]. The physical and chemical properties of ferropericlase should therefore have a major influence on the bulk properties of this entire region. Measurements of the sound velocities and elasticity of ferropericlase under relevant conditions are necessary to relate seismic observations in Earth's lower mantle to its mineralogy and chemistry, because seismic wave velocities directly probe Earth's deep mantle with high spatial resolution. The elastic properties investigated at high pressure of polycrystalline (Mg,Fe)O and $Fe_{1-x}O$-wüstite have been investigated using static compression [e.g., *Richet et al.*, 1989; *Fei et al.*, 1992; *Jacobsen et al.*, 2002, 2005; *Zhang and Kostak*, 2002; *van Westrenen et al.*, 2005; *Lin et al.*, 2005], nuclear resonant inelastic x-ray scattering [*Struzhkin et al.*, 2001], shock wave measurements [*Vassiliou and Ahrens*, 1982], and ultrasonic methods [*Jackson et al.*, 1978; *Bonczar and Graham*, 1982; *Kung et al.*, 2002]. In the last investigation the pressure dependencies of the adiabatic bulk and shear moduli as well as the sound velocities of ferropericlase were reported [*Kung et al.*, 2002]. The single-crystal elastic moduli of a suite of (Mg,Fe)O samples were reported at room-pressure conditions [*Jacobsen et al.*, 2002]. High-pressure shear wave velocity determinations were performed to ~8 GPa using gigahertz ultrasonic methods on single-crystals of (Mg,Fe)O with the following compositions: $(Mg_{0.760}Fe_{0.239}\square_{0.001})O$, $(Mg_{0.423}Fe_{0.541}\square_{0.036})O$, $(Mg_{0.211}Fe_{0.762}\square_{0.027})O$, and $(Fe_{0.946}\square_{0.054})O$, with $^{VI}\square$ vacancies (empty boxes denote a vacancy in a crystal structure) [*Jacobsen et al.*, 2004]. High-pressure Brillouin

[1]Department of Geology, University of Illinois, Urbana, Illinois, USA.
[2]Now at Division of Geological and Planetary Sciences, California Institute of Technology, Pasadena, California, USA.
[3]Now at HP-CAT, Advanced Photon Source, Argonne National Laboratory, Argonne, Illinois, USA.
[4]Geophysical Laboratory, Carnegie Institution of Washington, Washington, D. C., USA.
[5]Now at Department of Geological Sciences, Northwestern University, Evanston, Illinois, USA.
[6]GeoForschungsZentrum, Potsdam, Germany.
[7]Lunar and Planetary Institute, Houston, Texas, USA.

0148-0227/06/2005JB004052$09.00

scattering measurements have been performed to 9 GPa on a single-crystal of $(Mg_{0.987}Fe_{0.013})O$ (H. J. Reichmann et al., personal communication, 2006). Simultaneous high-pressure and high-temperature determinations of the single-crystal elasticity and aggregate acoustic properties of MgO have been carried out using ultrasonic methods [*Chen et al.*, 1997] and single-crystal first-principles calculations [*Karki et al.*, 1999], but no such investigations have thus far been reported for ferropericlase.

[3] Under ambient pressure-temperature conditions and at low iron concentrations, (Mg,Fe)O is characterized by high elastic anisotropy [*Jacobsen et al.*, 2002]. Therefore determinations of the single-crystal elasticity at relevant pressures and temperatures are necessary for the interpretation of observed seismic anisotropy in the lower mantle. However, the pressure dependence of the full elastic modulus tensor of ferropericlase remains unknown above 9 GPa. Here we report the full single-crystal elastic modulus tensor to 20 GPa for ferropericlase containing 6 mol% FeO, a composition close to the range of suggested ferropericlase compositions in Earth's lower mantle [*Irifune*, 1994; *Wood and Rubie*, 1996; *Mao et al.*, 1997; *Andrault*, 2001].

2. Experiment

[4] The ferropericlase sample used in this investigation is from the same bulk sample used by *Jacobsen et al.* [2002] for gigahertz ultrasonic interferometric measurements. The samples' synthesis, chemistry, structure, and elastic properties were characterized at room pressure and room temperature by *Jacobsen et al.* [2002]. Briefly, the ferropericlase crystal used in this study was synthesized by interdiffusion of iron and magnesium [e.g., *Mackwell et al.*, 2005], using an MgO single-crystal ($\sim 5 \times 5 \times 0.5$ mm^3) and a prereacted (Mg,Fe)O powder as the starting material. The ferric concentration was determined to be $Fe^{3+}/\Sigma Fe = 0.02 \pm 0.01$ by conventional Mössbauer spectroscopy measurements using the natural abundance of ^{57}Fe in the sample ($\sim$2.2%). Microprobe analyses show that the iron is homogeneously distributed at the sampling interval of about 10 μm, resulting in a chemical formula of $(Mg_{0.941}Fe_{0.058}\square_{0.001})O$ [*Jacobsen et al.*, 2002]. The NaCl (or B1) structure (space group *Fm*3*m*) was verified using single-crystal conventional X-ray diffraction, and a lattice parameter of, $a = 4.2190 \pm 0.0001$ Å, was obtained [*Jacobsen et al.*, 2002]. A density of 3.723 ± 0.008 g/cm^3 was calculated from the chemical analyses and the measured lattice parameter, correcting for the $^{VI}\square$ vacancies [*Jacobsen et al.*, 2002]. Hereafter we will refer to this sample as Fp06.

[5] A portion of the Fp06 cube was cleaved perpendicular to (100) and prepared for Brillouin scattering measurements. The Fp06 sample was polished on both sides with parallel faces to a thickness of 27 μm. The resulting platelet ($27 \times 200 \times 340$ μm^3) was mounted on a thin glass fiber that was fixed to a goniometer head for Brillouin measurements at room pressure. The sample has a light orange hue, so a low input laser power was used ($\sim$15 mW focused on the sample) in an effort to avoid local heating of the sample. This platelet was then unmounted, polished further to a thickness of 20 μm, and cut into smaller plates for high-pressure measurements.

[6] Analysis of the photon intensity as a function of frequency shift was obtained using a solid-state detector and a six-pass tandem Fabry Perot interferometer [*Sandercock*, 1982]. Details of the Brillouin system have been described previously [*Sinogeikin et al.*, 1998]. The sound velocities were calculated from the measured frequency shifts using the following relationship for a symmetric scattering geometry [*Whitfield et al.*, 1976]:

$$V_i = \left(\frac{\lambda_0 \Delta \upsilon_{B,i}}{2 \sin\left(\frac{\theta^*}{2}\right)} \right), \quad (1)$$

where V_i is the compressional ($V_{i=P}$) or shear ($V_{i=S}$) phonon velocity, $\Delta\nu_{B,i}$ is the corresponding measured Brillouin shift, λ_0 is the incident argon ion laser wavelength (λ_0 = 514.5 nm), and θ* is the angle between the incident and the scattered light outside the sample or diamond anvil cell (sometimes referred to as the external scattering angle). In the measurements presented here a 90° symmetric scattering geometry (θ* = 90°) was used at room pressure. At high pressures, either θ* = 80° or θ* = 50° was used depending on the diamond anvil cell (DAC) used (see below). In order to reduce systematic velocity errors, Brillouin measurements on an oriented single-crystal MgO standard were performed before the room-pressure and high-pressure measurements at all scattering geometries (θ* = 90°, 80°, and 50°). More detailed descriptions for high-pressure Brillouin scattering measurements have been explained elsewhere [e.g., *Zha et al.*, 1993, 1996; *Sinogeikin and Bass*, 2000].

[7] In all high-pressure measurements, methanol-ethanol-water (MEW) in a volume ratio of 16:3:1 was used as a pressure-transmitting medium. Ruby chips or spheres [*Chervin et al.*, 2001] were used as pressure markers using the calibrated ruby R_1 fluorescence line shift [*Mao et al.*, 1986] (see Table 1). The average pressure was determined from fluorescence measurements made on several rubies within the sample chamber before and after each Brillouin experiment. The uncertainties in pressure are given by the standard deviation of the pressures determined from all rubies in the sample chamber (see Table 1). Brillouin scattering is also highly sensitive to vignetting, a phenomenon that occurs when part of the scattered and/or incident light cone is blocked by the diamond supports and/or the gasket [*Oliver et al.*, 1992; *Sinogeikin and Bass*, 2000]. This was minimized by using a small aperture mask before the collecting lens. Vignetting was further minimized by choosing a large hole and opening for the diamond supports, having a sufficiently small ratio (less than 1:2) of the gasket thickness to the gasket hole diameter, and loading the sample such that it is in the center of the gasket hole.

[8] The first set of high-pressure experiments was performed using a Merrill-Bassett style three-screw DAC [*Merrill and Bassett*, 1974] with a large angular aperture (approximate full cone angle of 96°). The sample ($20 \times 100 \times 110$ μm^3) was loaded together with MEW and 7 ruby chips into a 235-μm-diameter hole that was drilled in a spring steel gasket preindented to a thickness of 100 μm. Although the angular opening in the DAC is large, a scattering geometry of 90° would result in vignetting [*Whitfield et al.*, 1976; *Sinogeikin and Bass*, 2000]. There-

Table 1. Density, Aggregate Acoustic Velocities, Single-Crystal Elastic Moduli, and Adiabatic Bulk and Shear Moduli for Fp06 As a Function of Pressure

P,[a] GPa	ρ, g/cm^3	V_P, km/s	V_S, km/s	C_{11}, GPa	C_{44}, GPa	C_{12}, GPa	K_S,[b] GPa	μ_{VRH},[b] GPa
				Outside DAC (θ = 90°)*				
0.0001	3.723(8)[c]	9.33(7)	5.70(5)	284(3)	147(1)	103(1)	163(3)	121(2)
				θ = 80° (MEW1)*				
4.4	3.820(8)	9.61(8)	5.79(5)	320(3)	148(1)	112(1)	181(4)	128(3)
9.5(1)	3.924(9)	9.90(8)	5.96(5)	364(4)	151(2)	117(1)	199(4)	139(3)
10.8(1)	3.950(9)	9.99(8)	6.04(5)	373(4)	156(2)	116(1)	202(4)	144(3)
13.3(4)	3.997(9)	10.13(8)	6.11(5)	396(4)	157(2)	119(1)	211(4)	149(3)
				θ = 50° (MEW2)*				
3.6	3.803(8)	9.54(8)	5.78(5)	313(3)	147(1)	109(1)	177(4)	127(3)
11.2(2)	3.957(9)	10.01(8)	6.02(5)	379(4)	153(2)	119(1)	206(4)	143(3)
15.2(6)	4.033(9)	10.25(8)	6.15(5)	413(4)	158(2)	124(1)	220(5)	152(3)
17.4(7)	4.073(9)	10.32(8)	6.19(5)	427(4)	160(2)	125(1)	225(5)	156(3)
20.2(10)	4.122(9)	10.49(8)	6.24(5)	450(5)	162(2)	134(1)	239(5)	160(3)
20.1(10)[d]	4.120(9)	10.52(9)	6.27(6)	452(5)	164(2)	134(1)	240(5)	162(3)
16.1(6)[d]	4.049(9)	10.29(8)	6.16(5)	418(4)	159(2)	126(1)	224(5)	154(3)
11.9(1)[d]	3.971(9)	10.03(8)	6.03(5)	381(4)	155(2)	121(1)	207(4)	144(3)

[a]Average pressure and associated uncertainties are reported from measurements made before and after each experiment. Uncertainties in pressure are determined from the standard deviation of the pressures calculated from the ruby fluorescence R_1 shift [*Mao et al.*, 1986] of up to seven rubies placed around the sample within the sample chamber.

[b]$K_S = 1/3(C_{11} + 2C_{12})$ and μ_{VRH} is the Voigt-Reuss-Hill average, where μ_{VRH} is the arithmetic mean of the Voigt and Reuss bounds: $\mu_V = 1/5(C_{11} - C_{12} + 3C_{44})$ and $\mu_R = 15[12/(C_{11} - C_{12}) + 9/C_{44}]^{-1}$ [*Watt et al.*, 1976].

[c]Room-pressure density is from *Jacobsen et al.* [2002].

[d]Measurements are taken on pressure decrease. The uncertainties in aggregate velocities, high-pressure densities, and C_{ij} are taken from the statistical (root-mean-square) errors from the fitting procedure of the data (see text). Error propagation was used to calculate the uncertainties for K_S and μ_{VRH}. All uncertainties are given in parentheses for the last significant digit(s).

fore Brillouin measurements were performed using an 80° symmetric scattering geometry (θ* = 80°) at pressures of 4.4, 9.5, 10.8, and 13.3 GPa. At higher pressures the gasket flowed, so the DAC was unloaded. The second set of experiments was performed using a symmetric piston-cylinder DAC with a 60° full angle-opening. An Fp06 sample with the dimensions of 20 × 40 × 79 μm^3 was loaded together with MEW and five ruby spheres into a 150-μm-diameter hole that was drilled in a rhenium gasket preindented to a thickness of 55 μm. A scattering geometry of 50° (θ* = 50°) was used, and data were collected on increasing pressure at 3.6, 11.2, 15.2, 17.4, and 20.2 GPa. Measurements were also taken on decreasing pressure at 20.1, 16.1, and 11.9 GPa. Selected representative Brillouin spectra are shown in Figure 1. Note that a high signal-to-noise ratio persists to the highest pressure achieved in this study (P = 20.2 GPa). The broadening of the Fp06 peaks at this pressure is likely owing to the observed pressure gradient within the sample chamber.

3. Results

[9] Three independent elastic moduli fully characterize the elasticity of Fp06 because it is cubic. Therefore measurements in two distinct directions (e.g., [001] and [011]) are the minimum requirements to constrain the three elastic moduli. Multiple crystallographic directions were sampled including redundant measurements at different settings on the three-circle goniometer to increase the precision of our results. All phonon directions were within the (100) plane. At each pressure, Brillouin spectra were collected in up to 14 directions over an angular range of 180°, separated by approximately 15° increments (Figure 2). The only exception to this occurred at pressures of 3.6 and 4.4 GPa, where the shear velocities of Fp06 near the [011] direction overlap with the compressional velocity of MEW. In some directions, two different spectra were collected with the laser focused on different areas of the sample; we found that these measured velocities were the same within the given uncertainties. In total, 42 mode velocities at room pressure and over 30 mode velocities for each high-pressure measurement were obtained.

[10] The velocities of acoustic phonons are related to the single-crystal elastic moduli through the Christoffel equation [*Musgrave*, 1970],

$$\det\left|C_{ijkl}n_j n_l - \rho V^2 \delta_{ik}\right| = 0, \tag{2}$$

where C_{ijkl} is the elastic modulus tensor, n_j and n_l are the unit vectors in the phonon propagation direction and the indices j and l are summed over, ρ is the density, V is phonon velocity, and δ_{ik} is the Kronecker delta (where δ_{ik} = 0 for $i \neq k$ and δ_{ik} = 1 for $i = k$). A linearized inversion method was used to solve the three independent elastic moduli (in reduced Voigt notation: C_{11}, C_{12}, and C_{44}) using the measured velocities as a function of crystallographic direction [*Weidner and Carleton*, 1977] and the ambient pressure density (ρ = 3.723(8) g/cm^3 [*Jacobsen et al.*, 2002]) as input for each pressure. The aggregate velocities (V_P and V_S) at each pressure are also an outcome of this inversion procedure and are independent of the assumed density. An iterative procedure described by *Sinogeikin and Bass* [2000] was then used to obtain the density, the adiabatic bulk (K_S) and shear (μ_S) moduli, and their pressure derivatives (K'_{0S} and μ'_{0S}) using a third-order finite strain equation of state (EOS) [*Davies and Dziewonski*, 1975]. A fit to all of the data yields a set of best fit densities (Table 1)

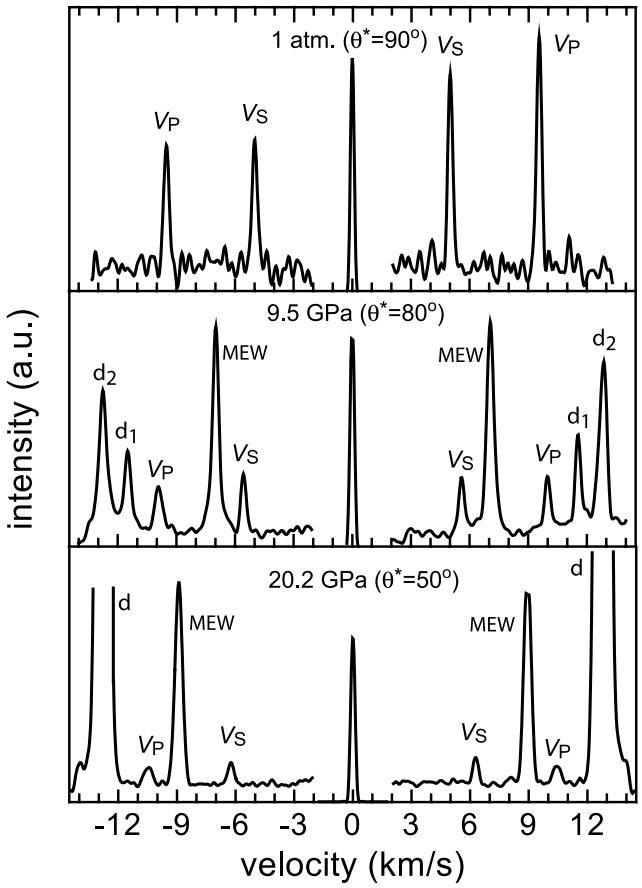

Figure 1. Representative Brillouin spectra at different pressures (1 atmosphere, 9.5 GPa, and 20.2 GPa) and at different scattering geometries (θ*) of Fp06 in approximately the [011] phonon direction within the (100) crystallographic plane. The 1 atm. spectrum was collected outside the DAC. The compressional (V_P) and shear (V_S) wave velocities of Fp06 are labeled, as well as the methanol-ethanol-water compressional wave velocity (MEW) and the diamond shear velocities (d_1, d_2). In all spectra, the peak corresponding to the reference energy (velocity = 0 km/s) has been scaled down. The intensity axes for each pressure are not equal; in the lower spectrum, the diamond peak intensities are larger than the scale shown. Direct conversion of the measured data (in units of GHz) to the horizontal scale shown here (velocity, in units of km/s) requires knowledge of the momentum transfer (i.e., the scattering angle) and is done using equation (1) (see text).

associated with the following pressure derivatives of the adiabatic bulk and shear moduli: $K'_{0S} = 3.9 \pm 0.2$ and $\mu'_{0S} = 2.1 \pm 0.1$. The uncertainties are obtained from the fitting procedure and therefore represent the statistical fluctuations of the data. The uncertainties in pressure are also included in these uncertainties. These results are summarized in Table 1 and shown in Figures 2–5. Using only the data up to 13.3 GPa (considered to be within the hydrostatic limit of MEW), one obtains: $K'_{0S} = 3.80 \pm 0.25$ and $\mu'_{0S} = 2.09 \pm 0.15$, values that are well within the uncertainties of those which were determined from the entire data set.

[11] Within the investigated pressure range, the aggregate acoustic velocities and single-crystal elastic moduli can be described using a linear relationship with pressure (Figures 3 and 4),

$$V_S(\text{km/s}) = 5.70(\text{km/s}) + 0.029 \times P(\text{GPa}), \quad (3)$$

$$V_P(\text{km/s}) = 9.33(\text{km/s}) + 0.058 \times P(\text{GPa}), \quad (4)$$

$$C_{11}(\text{GPa}) = 284(\text{GPa}) + 8.35 \times P(\text{GPa}), \quad (5)$$

$$C_{12}(\text{GPa}) = 103(\text{GPa}) + 1.42 \times P(\text{GPa}), \quad (6)$$

$$C_{44}(\text{GPa}) = 147(\text{GPa}) + 0.89 \times P(\text{GPa}). \quad (7)$$

The uncertainties for the pressure derivatives of the above-listed quantities are less than 5%. The uncertainties for the aggregate velocities, as well as C_{11}, C_{12}, and C_{44} are given in Table 1. At pressures beyond the range investigated here, the linear relationships (equations (3)–(6)) may not hold, considering the likely electronic spin crossover occurring in the iron component of ferropericlase at higher pressures [e.g., *Lin et al.*, 2005].

[12] At room pressure, we find that the addition of a small amount of iron in MgO causes a significant decrease in several quantities, such as the aggregate velocities (V_P and V_S), C_{11} and C_{44}, and the shear modulus. On the other hand, the density and C_{12} increases, and the bulk modulus remains

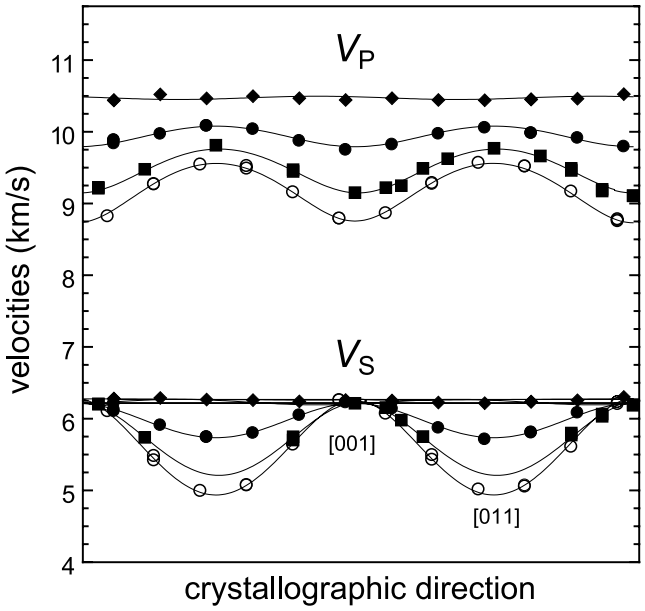

Figure 2. Compressional (V_P) and shear (V_S) wave velocities of Fp06 as a function of crystallographic direction in the (100) crystallographic plane for selected pressures: 1 atm. outside the DAC (open circles), 4.4 GPa (solid squares), 11.2 GPa (solid circles), and 20.2 GPa (solid diamonds). The uncertainties in velocities are less than the size of the symbols. The solid lines are calculated from the best fit single-crystal elastic moduli determined for each pressure displayed here.

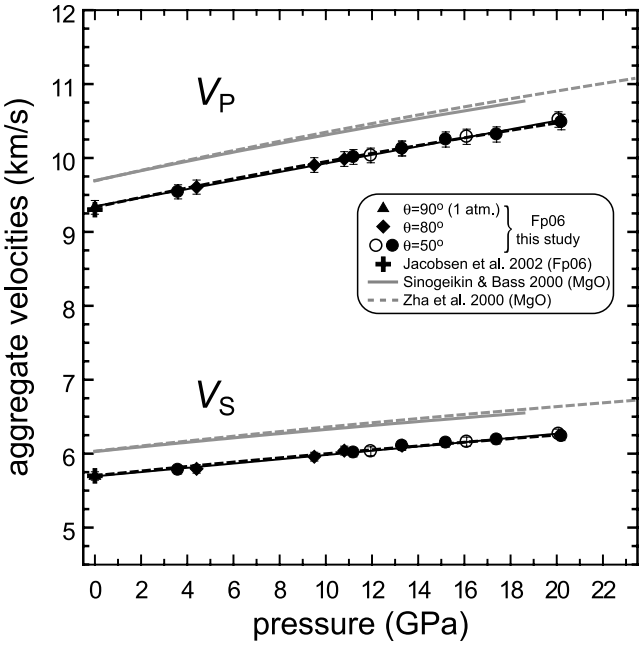

Figure 3. Aggregate compressional (V_P) and shear (V_S) wave velocities of Fp06 as a function of pressure at room temperature. Most symbols and lines are explained in the legend. The open circles are from data collected on pressure decrease. The solid black lines are linear fits to the data (equations (3) and (4); see text). The dashed black lines are calculated from the third-order finite-strain equation of state for aggregate V_P and V_S [*Davies and Dziewonski*, 1975] and are virtually indistinguishable from the linear fits. The black crosses are from room-pressure gigahertz ultrasonic measurements from the same bulk sample [*Jacobsen et al.*, 2002]. The gray lines are from Brillouin measurements on single-crystal MgO.

unchanged. These results are in excellent agreement with results obtained from gigahertz ultrasonic interferometry performed on the same bulk sample [*Jacobsen et al.*, 2002], thus demonstrating high interlaboratory precision between the two methods at room pressure.

4. Geophysical Implications

[13] Knowledge of the elastic anisotropy of ferropericlase at relevant pressures and temperatures may provide insight to the undetermined origins of seismic anisotropy within Earth, such as the core-mantle boundary region where ferropericlase is suggested to coexist with silicate perovskite or post-perovskite [*Gurnis et al.*, 1998; *Murakami et al.*, 2004; *Tsuchiya et al.*, 2004]. Elastic anisotropy is a measure of the variations in stiffness and sound velocity for different crystallographic directions in a given solid. For cubic material, the elastic anisotropy (A) can be expressed as the following [*Karki et al.*, 1999]:

$$A = \left[\frac{2C_{44} + C_{12}}{C_{11}}\right] - 1, \tag{8}$$

and is equal to zero for an elastically isotropic solid. At room pressure, our value of $A = 0.39 \pm 0.01$ (approximately 10% larger than that for MgO, as shown in Figure 6) (Table 2), is in excellent agreement with results obtained from gigahertz ultrasonic interferometry performed on the same bulk sample [*Jacobsen et al.*, 2002]. For comparison, $A \cong 0$ for FeO [*Jacobsen et al.*, 2002] at room pressure. At 20.2 GPa, we find that the anisotropy factor in Fp06 is approximately zero ($A = 0.02 \pm 0.03$) (Figures 2 and 6). If we compare the anisotropy-factor A of Fp06 with previous Brillouin data on MgO to 18.6 GPa [*Sinogeikin and Bass*, 2000] and to 54.7 GPa [*Zha et al.*, 2000], the data agree well for pressures below 20 GPa. A different expression of elastic anisotropy using sound velocities can be expressed as the following:

$$A_{V_{P,S}}(\%) = 100 \times \frac{V_{i,\max} - V_{i,\min}}{V_{i,VRH}}, \tag{9}$$

where V_i is V_P or V_S. At room pressure, the anisotropy for V_P is 8% and for V_S it is 22%; at 20.2 GPa, the anisotropies of V_P and V_S are 0%. Elasticity studies at high temperatures (room pressure) show that the elastic anisotropy in MgO increases with increasing temperature [*Sinogeikin et al.*, 2000]. Results from simultaneous high-pressure (to 8 GPa) and high-temperature (to 1600 K) ultrasonic experiments show that the cross derivatives $(d^2C_{ij})/(dPdT)$ are significant and suggest that under lower mantle conditions MgO remains elastically anisotropic [*Chen et al.*, 1997].

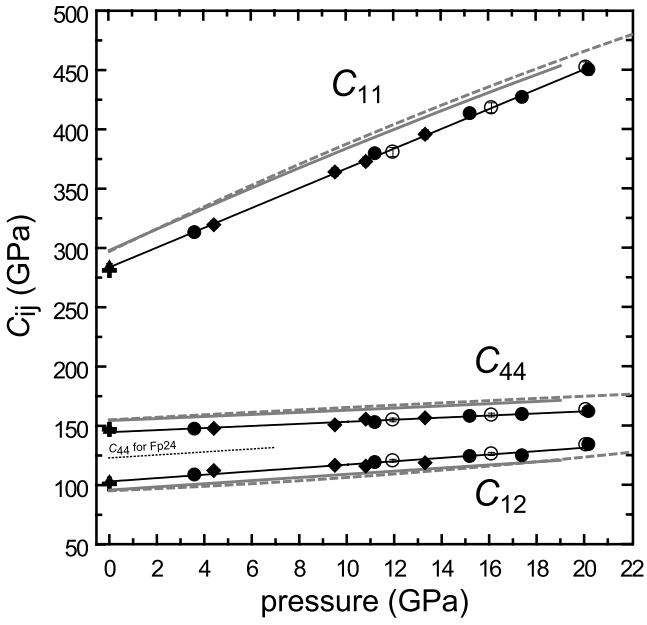

Figure 4. Single-crystal elastic moduli of Fp06 as a function of pressure at room temperature. The solid black lines are linear fits to data (equations (5), (6), and (7); see text). The gray solid and dashed lines are the second-order polynomial fits reported from the single-crystal MgO Brillouin measurements of *Sinogeikin and Bass* [2000] and *Zha et al.* [2000], respectively. The dotted black line is the pressure dependence of C_{44} for single-crystal $(Mg_{0.76}Fe_{0.24})O$ determined to ~7.5 GPa in a DAC using gigahertz ultrasonic interferometry [*Jacobsen et al.*, 2004]. The symbols have the same meaning as in Figure 3.

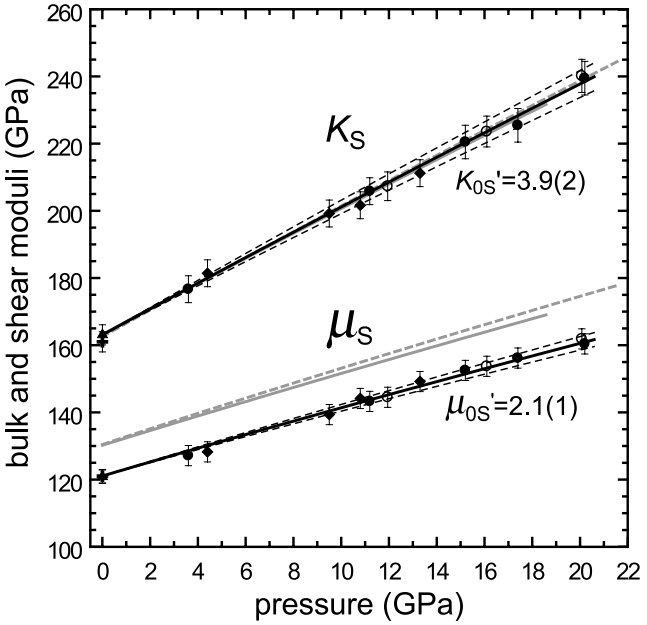

Figure 5. Adiabatic bulk (K_S) and shear ($\mu_S = \mu_{VRH}$) moduli of Fp06 as a function of pressure at room temperature. The solid black lines are calculated from a third-order finite-strain equation of state [*Davies and Dziewonski*, 1975], and the dashed black lines show the envelope of elastic moduli produced by the given uncertainties in K_{0S}' and μ_{0S}' (shown in parentheses in the figure). The symbols and lines have the same meaning as in Figure 3.

[14] The pressure derivatives of all Fp06 properties (with the exception of μ'_{0S}) are identical to those of MgO within experimental uncertainties [*Spetzler*, 1970; *Jackson and Niesler*, 1982; *Yoneda*, 1990; *Sinogeikin and Bass*, 2000; *Zha et al.*, 2000]. High-pressure shear wave velocity determinations were performed to ~7.5 GPa using gigahertz ultrasonic methods on single-crystal $(Mg_{0.760}Fe_{0.239}\square_{0.001})O$ (referred to here as Fp24) [*Jacobsen et al.*, 2004], which is close to the composition measured in this study. Although dC_{44}/dP for Fp24 is higher than dC_{44}/dP obtained for Fp06 (this study) (see Figure 4), the slopes are indistinguishable for pressures below 8 GPa.

[15] On the other hand, μ'_{0S} appears to show a systematic decreasing trend with increasing iron content. This observation has been recognized before [*Jackson et al.*, 1990], and is in agreement with recent high-pressure sound velocity determinations on polycrystalline $(Mg_{0.83}Fe_{0.17})O$ using ultrasonic interferometry in combination with synchrotron energy-dispersive X-ray diffraction [*Kung et al.*, 2002], and in agreement with high-pressure Brillouin scattering measurements on a single crystal of $(Mg_{0.987}Fe_{0.013})O$ (H. J. Reichmann et al., personal communication, 2006). The dependence of K'_{0S} and μ'_{0S} of ferropericlase for low iron concentrations determined from adiabatic measurements is plotted in Figure 7. *Jackson* [1998] performed an adiabatic decompression of the PREM model [*Dziewonski and Anderson*, 1981] for the lower mantle based on a finite strain fit to seismological data and determined that K'_S = 3.89 and μ'_S = 1.56 at some unknown high temperature at

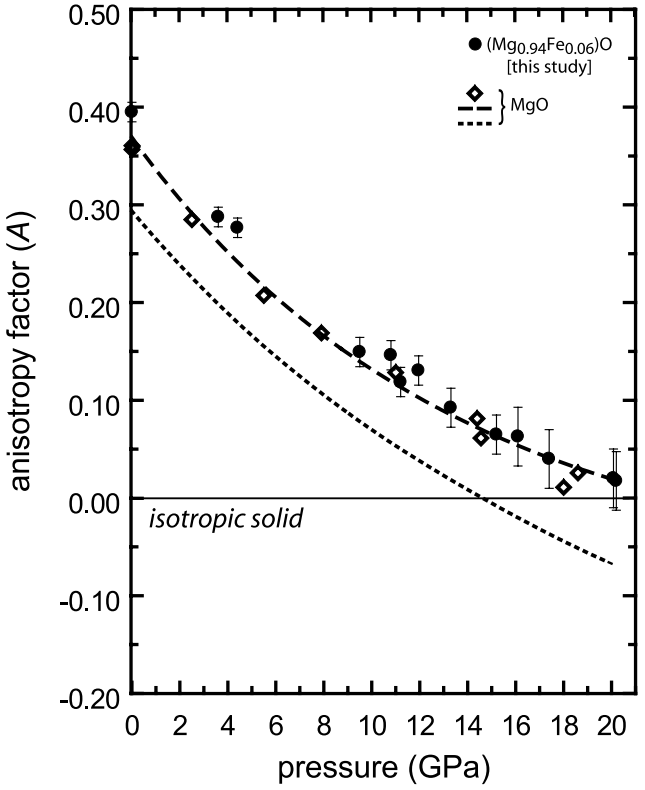

Figure 6. Anisotropy factor, expressed as: $A = [(2C_{44} + C_{12})/C_{11}] - 1$ [*Karki et al.*, 1999], of single-crystal ferropericlase (this study) and MgO as a function of pressure. Results from Fp06 (solid black spheres) are calculated directly from our measured C_{ij} in Table 1. The open diamonds are calculated from reported C_{ij} of MgO from measurements to 18.6 GPa [*Sinogeikin and Bass*, 2000], the long-dashed black line is the A factor calculated from the reported second-order polynomial expression of the C_{ij} of MgO from measurements to 54.7 GPa [*Zha et al.*, 2000], and the short-dashed black line is from theoretical calculations on MgO to over 100 GPa [*Karki et al.*, 1999].

Table 2. Some Physical Properties of Fp06[a]

P,[b] GPa	A[c]	C[d] (GPa)	Poisson Ratio[e]
0.0001	0.39	−44	0.203
4.4	0.28	−44	0.214
9.5(1)	0.15	−53	0.216
10.8(1)	0.15	−61	0.211
13.3(4)	0.09	−65	0.214
3.6	0.29	−46	0.210
11.2(2)	0.12	−56	0.218
15.2(6)	0.06	−64	0.219
17.4(7)	0.04	−70	0.219
20.2(10)	0.02	−68	0.226
20.1(10)[f]	0.02	−70	0.225
16.1(6)[f]	0.06	−65	0.220
11.9(1)[f]	0.13	−58	0.217

[a]Anisotropy factor (A), Cauchy violation (C), and Poisson ratio for Fp06 as a function of pressure.
[b]Same pressures as listed in Table 1.
[c]$A = [(2C_{44} + C_{12})/C_{11}] - 1$ [*Karki et al.*, 1999].
[d]Cauchy violation: $C_{12} - C_{44} - 2P$.
[e]Poisson ratio, $\nu = [(V_P/V_S)^2 - 2]/[2*((V_P/V_S)^2 - 1)]$.
[f]Measurements taken on pressure decrease.

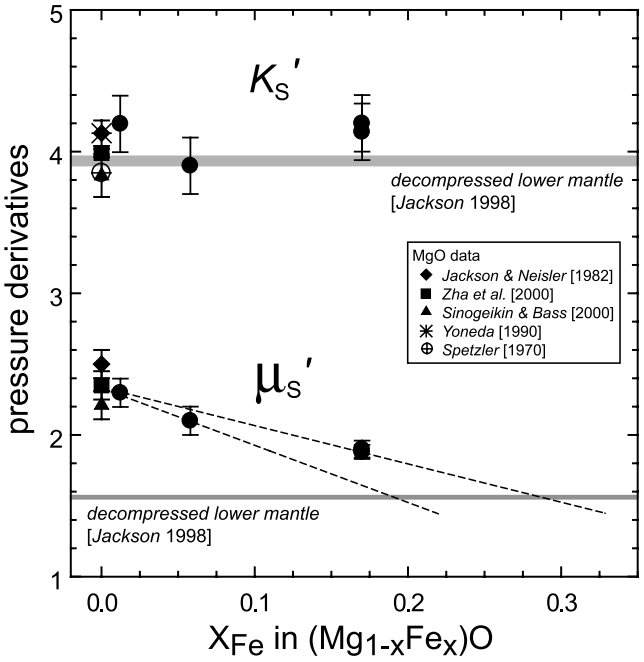

Figure 7. Room-pressure room temperature pressure derivatives of the adiabatic bulk and shear moduli of high-spin ferropericlase plotted as a function of iron content. The symbols for MgO are given in the legend. The data for X_{Fe} = 0.013, X_{Fe} = 0.06 and X_{Fe} = 0.17 are from H. J. Reichmann et al. (personal communication, 2006), this study, and *Kung et al.* [2002], respectively. The gray solid lines are the pressure derivatives of the adiabatic bulk and shear moduli (shading includes lower Reuss bound) for the decompression of the PREM model for the lower mantle at some unknown high temperature at the foot of the adiabat [see *Jackson*, 1998]. If μ_S' decreases linearly with iron concentration (as shown by the dashed extrapolated lines), then high-spin Fp could be within the compositional range of $0.18 \geq X_{Fe} \geq 0.28$ to provide a good match to seismic gradients given by PREM.

the foot of the adiabat. The value of K_S' from *Jackson* [1998] is in very good agreement with determinations of K_{0S}' from this study (see Figure 7) and other expected minerals in the lower mantle [*Fiquet et al.*, 2000; *Shim et al.*, 2000; *Sinogeikin and Bass*, 2000; *Kung et al.*, 2002; *Jackson et al.*, 2005]. On the other hand, a static compression study on single-crystals of $(Mg_{0.725}Fe_{0.268}\square_{0.007})O$, $(Mg_{0.423}Fe_{0.541}\square_{0.036})O$, and $(Mg_{0.211}Fe_{0.762}\square_{0.027})O$ to ~9 GPa produces values of $K'_{T0} \cong 5.5 \pm 0.2$, with the possibility that this high value reflects the behavior of less-stoichiometric (Mg,Fe)O [*Jacobsen et al.*, 2002]. The value for μ_S' from *Jackson* [1998] for the lower mantle is smaller than experimental determinations for ferropericlase (this study and *Kung et al.* [2002]) and aluminous $MgSiO_3$ perovskite [*Jackson et al.*, 2005]. There are several possible explanations for this mismatch. If μ'_S of ferropericlase indeed decreases linearly with iron concentration, then given the results of this study, *Kung et al.* [2002], and H. J. Reichmann et al. (personal communication, 2006), ferropericlase should be within the compositional range of $(Mg_{0.82}Fe_{0.18})O$ to $(Mg_{0.72}Fe_{0.28})O$ to provide a good match to seismic gradients given by PREM [*Dziewonski and Anderson*, 1981] or that there is a positive iron gradient in ferropericlase in the lower mantle, with the assumption that K'_S is not significantly affected by iron content. A strong temperature dependence of the pressure derivatives for shear properties is also a possible explanation.

[16] Another possibility is that the occurrence of a high-spin to low-spin crossover in the iron component of ferropericlase under lower mantle pressures and temperatures could cause a change in the physical and chemical properties of ferropericlase. This is not necessarily mutually exclusive with the above mentioned possibilities. In recent X-ray emission spectroscopy investigations of $(Mg_{0.83}Fe_{0.17})O$ [*Badro et al.*, 2003] and $(Mg_{0.75}Fe_{0.25})O$ [*Lin et al.*, 2005] ferropericlase, a high- to-low-spin crossover was observed in the pressure range of 60 to 70 GPa and 54 to 67 GPa, respectively, at room temperature. Inferences from the volume versus pressure trend suggest that the bulk sound velocity of Fp would increase at the crossover pressure at room temperature [*Lin et al.*, 2005]. However, there is no information on the behavior of the shear elasticity or its pressure derivative at pressures above the crossover. Further, the high-temperature nature of this crossover has yet to be understood, but recent predictions [*Sturhahn et al.*, 2005] suggest that at temperatures close to an expected geotherm [*Brown and Shankland*, 1981], the pressure interval over which this crossover occurs may be approximately 30 GPa (~700 km). Any changes in physical and chemical properties would also be expected to be gradual. Therefore measurements to determine these changes in properties of ferropericlase across the spin crossover at high pressure and at appropriate lower mantle temperatures would be imperative for future geophysical modeling of Earth's deep mantle.

[17] **Acknowledgments.** We would like to thank C. Sanchez-Valle, W. Sturhahn, W.-P. Chen, X. Song, D. L. Lakshtanov, M. Roskosz, and J.-F. Lin for helpful discussions. Our manuscript benefited from comments made by I. Jackson and an anonymous reviewer. This research was funded in part by National Science Foundation grants EAR 0003383 (J. D. B.) and The Elasticity Grand Challenge project (EAR 0135642, to J. D. B.). J. M. J. also acknowledges the support of the MSA Grant for Student Research in Mineralogy and Petrology and a Carnegie Fellowship. S. D. J. is supported by NSF EAR-0440112, CDAC, and by a Carnegie Fellowship.

References

Anderson, D. L., and J. D. Bass (1986), Transition region of the Earth's upper mantle, *Nature*, *320*, 321–328.

Andrault, D. (2001), Evaluation of (Mg,Fe) partitioning between silicate perovskite and magnesiowustite up to 120 GPa and 2300 K, *J. Geophys. Res.*, *106*(B2), 2079–2087.

Badro, J., G. Fiquet, F. Guyot, J.-P. Rueff, V. V. Struzhkin, G. Vanko, and G. Monaco (2003), Iron partitioning in Earth's lower mantle: Toward a deep lower mantle discontinuity, *Science*, *300*, 789–791.

Bonczar, L. J., and E. K. Graham (1982), The pressure and temperature dependence of the elastic properties of polycrystal magnesiowustite, *J. Geophys. Res.*, *87*(B2), 1061–1078.

Brown, J. M., and T. J. Shankland (1981), Thermodynamic parameters in the Earth as determined from seismic profiles, *Geophys. J. Astron. Soc.*, *66*, 579–596.

Chen, G., R. C. Liebermann, and D. J. Weidner (1997), Elasticity of single-crystal MgO to 8 gigapascals and 1600 kelvin, *Science*, *280*, 1913–1916.

Chervin, J. C., B. Canny, and M. Mancinelli (2001), Ruby-spheres as pressure gauge for optically transparent high pressure cells, *High Pressure Res.*, *21*, 305–314.

Davies, G. F., and A. M. Dziewonski (1975), Homogeneity and constitution of the Earth's lower mantle and outer core, *Phys. Earth Planet. Inter.*, *10*, 336–343.

Dziewonski, A. M., and D. L. Anderson (1981), Preliminary Reference Earth Model, *Phys. Earth Planet. Inter.*, *25*, 297–356.

Fei, Y., H.-K. Mao, J. Shu, and J. Hu (1992), P-V-T equation of state of magnesiowustite ($Mg_{0.6}Fe_{0.4}$)O, *Phys. Chem. Miner.*, *18*, 416–422.

Fiquet, G., A. Dewaele, D. Andrault, M. Kunz, and T. Le Bihan (2000), Thermoelastic properties and crystal structure of $MgSiO_3$ perovskite at lower mantle pressure and temperature conditions, *Geophys. Res. Lett.*, *27*, 21–24.

Gurnis, M., M. E. Wysession, E. Knittle, and B. A. Buffett (1998), *The Core-Mantle Boundary Region*, *Geodyn. Ser.*, vol. 28, edited by M. Gurnis et al., 334 pp., AGU, Washington, D. C.

Irifune, T. (1994), Absence of an aluminous phase in the upper part of the Earth's lower mantle, *Nature*, *370*, 131–133.

Jackson, I. (1998), Elasticity, composition and temperature of the Earth's lower mantle: A reappraisal, *Geophys. J. Int.*, *134*, 291–311.

Jackson, I., and H. Niesler (1982), The elasticity of periclase to 3 GPa and some geophysical implications, in *High Pressure Research in Geophysics*, edited by S. Akimoto and M. H. Manghnani, pp. 93–113, Cent. of Acad. Publ., Tokyo.

Jackson, I., R. C. Liebermann, and A. E. Ringwood (1978), The elastic properties of (Mg_xFe_{1-x})O solid solutions, *Phys. Chem. Miner.*, *3*, 11–31.

Jackson, I., S. K. Khanna, A. Revcolevschi, and J. Berthon (1990), Elasticity, shear-mode softening and high-pressure polymorphism of wüstite ($Fe_{1-x}O$), *J. Geophys. Res.*, *95*(B13), 21,671–21,685.

Jackson, J. M., J. Zhang, J. Shu, S. V. Sinogeikin, and J. D. Bass (2005), High-pressure sound velocities and elasticity of aluminous MgSiO3 perovskite to 45 GPa: Implications for lateral heterogeneity in Earth's lower mantle, *Geophys. Res. Lett.*, *32*, L21305, doi:10.1029/2005GL023522.

Jacobsen, S. D., H.-J. Reichmann, H. A. Spetzler, S. J. Mackwell, J. R. Smyth, R. J. Angel, and C. A. McCammon (2002), Structure and elasticity of single-crystal (Mg,Fe)O and a new method of generating shear waves for gigahertz ultrasonic interferometry, *J. Geophys. Res.*, *107*(B2), 2037, doi:10.1029/2001JB000490.

Jacobsen, S. D., H. Spetzler, H.-J. Reichmann, and J. R. Smyth (2004), Shear waves in the diamond-anvil cell reveal pressure-induced instability in (Mg,Fe)O, *Proc. Natl. Acad. Sci. U. S. A.*, *101*(16), 5867–5871.

Jacobsen, S. D., J.-F. Lin, R. J. Angel, G. Shen, V. Prakapenka, P. Dera, H.-K. Mao, and R. J. Hemley (2005), Single-crystal synchrotron X-ray diffraction study of wüstite and magnesiowüstite at lower-mantle pressures, *J. Synchrotron Radiat.*, *12*, 577–583.

Karki, B. B., R. M. Wentzcovitch, S. de Gironcoli, and S. Baroni (1999), First-principles determination of elastic anisotropy and wave velocities of MgO at lower mantle conditions, *Science*, *286*, 1705–1707.

Knittle, E., and R. Jeanloz (1987), Synthesis and equation of state of $(Mg,Fe)SiO_3$ perovskite to over 100 gigapascals, *Science*, *235*, 668–670.

Kung, J., B. Li, D. J. Weidner, J. Zhang, and R. C. Liebermann (2002), Elasticity of ($Mg_{0.83}$,$Fe_{0.17}$)O ferropericlase at high pressure: Ultrasonic measurements in conjunction with X-radiation techniques, *Earth Planet. Sci. Lett.*, *203*, 557–566.

Lin, J.-F., V. V. Struzhkin, S. D. Jacobsen, M. Hu, P. Chow, J. Kung, H. Liu, H.-K. Mao, and R. J. Hemley (2005), Spin transition of iron in magnesiowüstite in the Earth's lower mantle, *Nature*, *436*, 377–380.

Mackwell, S. J., M. Bystricky, and C. Sproni (2005), Fe–Mg interdiffusion in (Mg,Fe)O, *Phys. Chem. Miner.*, *32*, 418–425, doi:10.1007/s00269-005-0013-6.

Mao, H.-K., J. Xu, and P. M. Bell (1986), Calibration of the ruby pressure gauge to 800-kbar under quasi-hydrostatic conditions, *J. Geophys. Res.*, *91*(B5), 4673–4676.

Mao, H.-K., G. Shen, and R. J. Hemley (1997), Multivariable dependence of Fe-Mg partitioning in the lower mantle, *Science*, *278*, 2098–2100.

Merrill, L., and W. A. Bassett (1974), Miniature diamond anvil pressure cell for single crystal X-ray diffraction studies, *Rev. Sci. Instrum.*, *45*, 290–294.

Murakami, M., K. Hirose, N. Kawamura, N. Sata, and Y. Onishi (2004), Post-perovskite phase transition in $MgSiO_3$, *Science*, *304*, 855–858.

Musgrave, M. J. P. (1970), *Crystal Acoustics: Introduction to the Study of Elastic Waves and Vibrations in Crystals*, Holden-Day, Boca Raton, Fla.

Oliver, W. F., C. A. Herbst, S. M. Lindsay, and G. H. Wolf (1992), A general method for determination of Brillouin linewidths by correction for instrumental effects and aperture broadening: Application to high-pressure diamond anvil cell experiments, *Rev. Sci. Instrum.*, *63*, 1884–1895.

Richet, P., H.-K. Mao, and P. M. Bell (1989), Bulk moduli of magnesiowustite from static compression experiments, *J. Geophys. Res.*, *94*(B3), 3037–3045.

Sandercock, J. R. (1982), Trends in Brillouin scattering: studies of opaque materials, supported films, and central modes, in *Topics in Applied Physics—Light Scattering in Solids III: Recent Results*, edited by M. Cardona, and G. Guntherodt, pp. 173–206, Springer, New York.

Shim, S.-H., T. S. Duffy, and G. Shen (2000), The stability and P-V-T equation of state for $CaSiO_3$ perovskite in the Earth's lower mantle, *J. Geophys. Res.*, *105*(B11), 25,955–25,968.

Sinogeikin, S. V., and J. D. Bass (2000), Single-crystal elasticity of pyrope and MgO to 20 GPa by Brillouin scattering in the diamond cell, *Phys. Earth Planet. Inter.*, *120*, 43–62.

Sinogeikin, S. V., T. Katsura, and J. D. Bass (1998), Sound velocities and elastic properties of Fe-bearing wadsleyite and ringwoodite, *J. Geophys. Res.*, *103*(B9), 20,819–20,825.

Sinogeikin, S. V., J. M. Jackson, B. O'Neill, J. W. Palko, and J. D. Bass (2000), Compact high-temperature cell for Brillouin scattering measurements, *Rev. Sci. Instrum.*, *71*, 201–206.

Spetzler, H. (1970), Equation of state of polycrystalline and single-crystal MgO to 8 kilobars and 800 K, *J. Geophys. Res.*, *75*(11), 2073–2087.

Struzhkin, V. V., et al. (2001), Nuclear inelastic X-ray scattering of FeO to 48 GPa, *Phys. Rev. Lett.*, *87*(25), 255501.

Sturhahn, W., J. M. Jackson, and J.-F. Lin (2005), The spin state of iron in minerals of Earth's lower mantle, *Geophys. Res. Lett.*, *32*, L12307, doi:10.1029/2005GL022802.

Tsuchiya, T., J. Tsuchiya, K. Umemoto, and R. M. Wentzcovitch (2004), Elasticity of post-perovskite $MgSiO_3$, *Geophys. Res. Lett.*, *31*, L14603, doi:10.1029/2004GL020278.

van Westrenen, W., et al. (2005), Thermoelastic properties of ($Mg_{0.64}Fe_{0.36}$)O ferropericlase based on in situ X-ray diffraction to 26.7 GPa and 2173 K, *Phys. Earth Planet. Inter.*, *151*, 163–176.

Vassiliou, M. S., and T. J. Ahrens (1982), The equation of state of $Mg_{0.6}Fe_{0.4}O$ to 200 GPa, *Geophys. Res. Lett.*, *9*, 127–130.

Watt, P. J., G. F. Davies, and R. J. O'Connell (1976), The elastic properties of composite materials, *Rev. Geophys.*, *14*(4), 541–563.

Weidner, D. J., and H. R. Carleton (1977), Elasticity of coesite, *J. Geophys. Res.*, *82*(B8), 1334–1346.

Whitfield, C. H., E. M. Brody, and W. A. Bassett (1976), Elastic moduli of NaCl by Brillouin scattering at high pressure in a diamond anvil cell, *Rev. Sci. Instrum.*, *47*, 942–947.

Wood, B. J., and D. C. Rubie (1996), The effect of alumina on phase transformations at the 660-kilometer discontinuity from Fe-Mg partitioning experiments, *Science*, *273*, 1522–1524.

Yoneda, A. (1990), Pressure derivatives of elastic constants of single crystal MgO and $MgAl_2O_4$, *J. Phys. Earth*, *38*, 19–55.

Zha, C.-S., T. S. Duffy, H.-K. Mao, and R. J. Hemley (1993), Elasticity of hydrogen to 24 GPa from single-crystal Brillouin scattering and synchrotron x-ray diffraction, *Phys. Rev. B*, *48*, 9246–9255.

Zha, C.-S., T. S. Duffy, R. T. Downs, H.-K. Mao, and R. J. Hemley (1996), Sound velocity and elasticity of single-crystal forsterite to 16 GPa, *J. Geophys. Res.*, *101*(B8), 17,535–17,546.

Zha, C.-S., H.-K. Mao, and R. J. Hemley (2000), Elasticity of MgO and a primary pressure scale to 55 GPa, *Proc. Natl. Acad. Sci.*, *97*(25), 13,494–13,499.

Zhang, J., and P. Kostak (2002), Thermal equation of state of magnesiowustite ($Mg_{0.6}Fe_{0.4}$)O, *Phys. Earth Planet. Inter.*, *129*, 301–311.

J. D. Bass, Department of Geology, University of Illinois, 1301 West Green Street, Urbana, IL 61801, USA. (jaybass@uiuc.edu)

J. M. Jackson, Division of Geological and Planetary Sciences, California Institute of Technology, 1200 East California Boulevard, Pasadena, CA, 91125, USA. (jackson@gps.caltech.edu)

S. D. Jacobsen, Department of Geological Sciences, Northwestern University, Evanston, IL, 60208, USA. (steven@earth.northwestern.edu)

S. J. Mackwell, Lunar and Planetary Institute, 3600 Bay Area Boulevard, Houston TX, 77058, USA. (mackwell@lpi.usra.edu)

H. J. Reichmann, GeoForschungsZentrum, Telegrafenberg, D-14473 Potsdam, Germany. (hanni@gfz-potsdam.de)

S. V. Sinogeikin, HP-CAT, Advanced Photon Source, Argonne National Laboratory, 9700 South Cass Avenue, Argonne, IL 60439, USA. (ssinog@hpcat.aps.anl.gov)